Effects of Regulated Expression of Mutant RhoA and Rac1 Small GTPases on the Development of Epithelial (MDCK) Cell Polarity

Tzuu-Shuh Jou and W. James Nelson

Department of Molecular and Cellular Physiology, Stanford University School of Medicine, Stanford, California 94305-5345

Abstract. MDCK cells expressing RhoA or Rac1 mutants under control of the tetracycline repressible transactivator were used to examine short-term effects of known amounts of each mutant before, during, or after development of cell polarity. At low cell density, Rac1V12 cells had a flattened morphology and intact cell–cell contacts, whereas Rac1N17 cells were tightly compacted. Abnormal intracellular aggregates formed between Rac1N17, F-actin, and E-cadherin in these nonpolarized cells. At all subsequent stages of polarity development, Rac1N17 and Rac1V12 colocalized with E-cadherin and F-actin in an unusual beaded pattern at lateral membranes. In polarized cells, intracellular aggregates formed with Rac1V12, F-actin, and an apical membrane protein (GP135). At low cell density, RhoAV14 and RhoAN19 were localized in the cytoplasm, and cells were generally flattened and more fibroblastic than epithelial in morphology. In polarized RhoAV14 cells, F-actin was diffuse at lateral membranes and prominent in stress fibers on the basal membrane. GP135 was abnormally localized to the lateral membrane and in intracellular aggregates, but E-cadherin distribution appeared normal. In RhoAN19 cells, F-actin, E-cadherin, and GP135 distributions were similar to those in controls. Expression of either RhoAV14 or RhoAN19 in Rac1V12 cells disrupted Rac1V12 distribution and caused cells to adopt the more fibroblastic, RhoA mutant phenotype. We suggest that Rac1 and RhoA are involved in the transition of epithelial cells from a fibroblastic to a polarized structure and function by direct and indirect regulation of actin and actin-associated membrane protein organizations.

Key words: GTPases • RhoA• cell polarity • cell adhesion • membrane domains

THE RhoA family of proteins, consisting of RhoA, Rac1, and Cdc42 subfamilies, are relatives of the small GTP-binding protein Ras (Hall, 1998). Like Ras, RhoA GTPases cycle between an active GTP-bound state and an inactive GDP-bound state (Bourne, 1993; Hall, 1998). Transitions between GTP- and GDP-bound forms of small GTPases are controlled by specialized regulators (Bourne, 1993). By cycling between GTP- and GDP-bound states, RhoA family GTPases transduce signals from cell surface receptors to intracellular target molecules (Hall, 1998).

Microinjection of dominant-active or dominant-negative RhoA GTPases revealed that each subfamily regulates, in a hierarchical manner, the formation and organization of specialized actin membrane structures in Swiss 3T3 fibroblasts (Hall, 1998). Cdc42 regulates filopodia formation, Rac1 controls lamellipodia and membrane ruffling, and RhoA is involved in the assembly and organization of stress fibers and focal adhesions (Ridley and Hall, 1992; Ridley et al., 1992; Nobes and Hall, 1995; Hall, 1998). These initial studies in fibroblasts have been extended to show that RhoA GTPases are involved in many other biological processes, including cell shape, cell motility, endocytosis, exocytosis, cell–substratum adhesion, and cytokinesis, all of which may involve RhoA GTPase control of actin-based structures (Symons, 1996; Burridge et al., 1997; Hall, 1998).

How RhoA GTPases regulate actin membrane structures is not well understood. Several downstream effectors of RhoA have been identified, including Rho-activated serine/threonine kinases (termed Rho-kinase, ROKα and ROKβ, and p160ROCK; Leung et al., 1995, 1996; Ishizaki et al., 1996; Matsui et al., 1996), which have pointed to a role of RhoA GTPases in regulating actinomyosin–based contractility. Rho-kinases phosphorylate both the regulatory subunit of the myosin phosphatase and the regulatory myosin light chain (Amano et al., 1996; Kimura et al., 1996). These activities cause an increase in myosin light chain phosphorylation and, thereby, promote a conformational change in myosin II that leads to bipolar filament formation and stimulate myosin ATPase activity (Burr-

Address all correspondence to W. James Nelson, Department of Molecular and Cellular Physiology, Stanford University School of Medicine, Beckman Center, B121, Stanford, CA 94305-5345. Tel.: (650) 725-7596. Fax: (650) 498-5286. E-mail: wjnelson@leland.stanford.edu

© The Rockefeller University Press, 0021-9525/98/07/85/16 $2.00

idge and Chrzanowska, 1996). Conformational changes in myosin II and myosin ATPase activity are required for the interaction of myosin with actin filaments and subsequent force generation. Another downstream effector of RhoA GTPases may be phosphatidylinositol 4-phosphate 5-kinase (Chong et al., 1994), which regulates phosphatidylinositol (4,5)-bisphosphate (PIP_2)[1] synthesis. PIP_2 has broad effects on the actin cytoskeleton, including binding to actin-monomer binding proteins (e.g., profilin), which results in release of actin monomers (Lassing and Lindberg, 1985; Goldschmidt et al., 1990), and causing the dissociation of capping proteins (e.g., gelsolin) from the ends of actin filaments (Fukami et al., 1992). Recently, the ezrin-radixin-moesin (ERM) family of actin-associated proteins (Matsui et al., 1998) and adducin (Kimura et al., 1998) have also been shown to be substrates for Rho-kinase. In general, all of these activities are likely to lead to promotion of actin filament assembly (Burridge et al., 1997).

These studies have provided important insights into the functions of RhoA GTPases in single, motile cells, but little is known about the role of RhoA GTPases in the structural and functional organization of epithelial cells, which interact to form organs and tissues. Studies in *Drosophila* indicate that Rac1 and Cdc42 regulate several aspects of epithelial cell organization in the imaginal disc, including cell survival, apico–basal epithelial elongation, and actin organization at cell–cell contacts and at the base of cells (Eaton et al., 1995). Other studies have focused on roles of RhoA GTPases in epithelial cells in vitro. In one study, it was reported that microinjection of RhoA or Rac1 mutants into keratinocytes disrupted E-cadherin–dependent cell–cell adhesion (Braga et al., 1997). Another study showed that expression of C3 exoenzyme, which ADP ribosylates and inactivates RhoA, disrupted tight junction organization and function in T84 intestinal epithelial cells, but did not affect cell–cell interactions (Nusrat et al., 1995). In contrast to those studies, it was reported recently that RhoA or Rac1 mutants had little or no effect on either cell–cell adhesion or tight junction organization in MDCK cells, except during PKC-induced TJ assembly in the presence of low extracellular calcium concentrations (Takaishi et al., 1997). The reason for the differences in these results and conclusions is unclear.

During the course of the in vitro studies described above, we were generating MDCK cell lines that expressed constitutively active or dominant-negative Rac1 or RhoA under the control of the tetracycline repressible transactivator (Gossen and Bujard, 1992). This expression system has some advantages over microinjection, in which the amount of protein expression is difficult to adjust and analysis is confined to a small number of cells, and stably transfected cell lines in which a fixed amount of protein is constitutively expressed. Using tetracycline repressible expression, we have been able to examine short-term effects of known amounts of RhoA mutants before, during, or after development of cell polarity. As controls, we used either the same cell population grown in the presence of doxycycline (DC) to repress RhoA mutant expression, or added back DC to RhoA mutant expressing cells to examine the reversibility of disrupted cellular processes. Here we report the characterization of these cells and show that RhoA and Rac1 are involved at multiple levels in the development of epithelial cell polarity; in the accompanying study (Jou et al., 1998), we describe in detail the roles of RhoA GTPases in regulating the structure and function of the epithelial tight junction.

1. *Abbreviations used in this paper*: DC, doxycycline; ERM, ezrin-radixin-moesin; PIP_2, phosphatidylinositol (4,5)-bisphosphate.

Materials and Methods

Plasmid Construction and Selection of MDCK Cell Lines Stably Expressing Mutant Small GTPases

pUMRhoAV14, pUMRhoAN19, pUMRac1V12, and pUMRac1N17, which express NH_2-terminal myc-tagged constitutively active RhoA, dominantly negative RhoA, constitutively active Rac1, and dominantly negative Rac1, respectively, were generously provided by Dr. Rong-Guo Qiu (Qiu et al., 1995*a*,*b*).

The parental MDCK T23 clone, which expresses the tetracycline-repressible transactivator (Barth et al., 1997), was used to generate stable lines expressing constitutively active and dominant-negative RhoA and Rac1. Using lipofectamine (GIBCO BRL, Gaithersburg, MD), parental T23 cells were cotransfected with expression vectors for small GTPase mutants (pUMRhoAV14, pUMRhoAN19, pUMRac1V12, and pUMRac1N17) and pHMR272, which carries the hygromycin resistance gene (Gossen and Bujard, 1992). In brief, 0.5 μg of cesium chloride density gradient purified mutant GTPase plasmid, 0.025 μg pHMR272, and 5 μl lipofectamine reagent were mixed in 200 μl of serum-free DME at room temperature for 45 min. The mixture was diluted with 800 μl serum-free DME and added to T23 MDCK cells in six-well cluster plates; cells were in log phase growth and had been incubated in 20 ng/ml DC (Sigma Chemical Co., St. Louis, MO) for at least 48 h before transfection. After 9 h at 37°C, the medium was replaced with DME containing 10% FBS (Gemini BioProducts, Calabasas, CA) and 20 ng/ml DC, and the cells were incubated for a further 24 h. The cells were then passaged to P-150 plates in medium containing 200 μg/ml hygromycin B (Calbiochem-Novabiochem Corp., La Jolla, CA). After selection for 10 d, surviving colonies were isolated using cloning rings, and mutant GTPase expression was assessed by either Western blotting or immunofluorescence 36 h after removal of DC. Positive clones were expanded in the presence of DC, aliquoted, and stored in liquid nitrogen. Parental T23 cells were also transfected with the empty pUHD10-3 vector and pHMR 272; eight clones were picked and pooled together to form the mock transfection control (pUHD).

Cell Culture

Parental T23 cells and transfected cells were grown in DME containing 10% FBS and 20 ng/ml DC at 37°C in a humidified atmosphere containing 5% CO_2. Cultures were routinely monitored for Mycoplasma infection. Generally, maximum expression of mutant genes occurred 36 to 48 h (RhoAV14, Rac1V12, Rac1N17) or >48 h (RhoAN19) after removal of DC from the culture medium. In calcium switch experiments, control and mutant small GTPase-expressing cells were grown in the presence or absence of 20 ng/ml DC at low density, trypsinized, and plated onto Transwell™ filters in medium containing 5 μM calcium (LCM) with or without 20 ng/ml DC. Cells were incubated in LCM for 4 h, gently rinsed twice in prewarmed LCM, and then incubated in DME/FBS containing 1.8 mM calcium (HCM) with or without 20 ng/ml DC.

Antibodies

The following antibodies were used: rabbit polyclonal anti–myc antibody (Santa Cruz Biotechnology, Inc., Santa Cruz, CA); mouse anti–myc hybridoma 9E10 (Dr. Gordon Cann, Stanford University Medical School, Stanford, CA); mouse anti–GP135 hybridoma 3F2/D8 (Dr. George K. Ojakian, SUNY Health Science Center, Brooklyn, NY); mouse anti–Rac1, E-cadherin, α-catenin, and β-catenin antibody (Transduction Laboratories, Lexington, KY); mouse anti–RhoA antibody (Santa Cruz Biotechnology, Inc.); mouse anti–Glu-Glu hybridoma supernatant was a gift from Dr. Marc Symons (Onyx Pharmaceuticals, Richmond, CA); rabbit polyclonal anti–E-cadherin antibody was a gift from Dr. James Marrs (In-

diana University School of Medicine, Indianapolis, IN; Marrs et al., 1993); rhodamine-conjugated phalloidin (Molecular Probes, Eugene, OR); rabbit polyclonal anti–rab11 antibody (Zymed Laboratories Inc., South San Francisco, CA); and affinity-purified fluorescein- and rhodamine-labeled secondary antibodies (Jackson ImmunoResearch Laboratories, Inc., West Grove, PA).

Immunofluorescence Microscopy

Confluent monolayers of MDCK cells were grown on rat tail collagen-coated coverslips or Transwell™ filters (Corning Costar, Cambridge, MA) in DME/FBS with or without 20 ng/ml DC. Cells were washed twice with Dulbecco's PBS (0.9 mM $CaCl_2$, 2.7 mM KCl, 1.5 mM KH_2PO_4, 0.5 mM $MgCl_2$, 137 mM NaCl, and 8.1 mM Na_2HPO_4) and then fixed for 20 min at room temperature in 3.7% paraformaldehyde in Dulbecco's PBS. Cells were then washed twice in Dulbecco's PBS at room temperature for 10 min and extracted with CSK buffer (50 mM NaCl, 300 mM sucrose, 10 mM Pipes, pH 6.8, 3 mM $MgCl_2$, 0.5% [vol/vol] Triton X-100) at room temperature for 10 min. Cells were washed twice in Dulbecco's PBS at room temperature for 10 min. Cells were blocked in Dulbecco's PBS containing 1% BSA, 10% goat serum, and 50 mM NH_4Cl for 1 h at room temperature or overnight at 4°C. After blocking, cells were washed briefly in Dulbecco's PBS and 0.2% BSA and then incubated in primary antibody solution for 1 h at room temperature or overnight at 4°C. Cells were then washed three times in Dulbecco's PBS and 0.2% BSA and incubated in fluorescein- or rhodamine-conjugated goat secondary antibody solution for 1 h at room temperature. Cells were washed three times in Dulbecco's PBS and 0.2% BSA and mounted in either Elvanol (16.7% Mowiol, 33% glycerol, 0.1% phenylenediamine) or Vectashield (Vector Laboratories, Inc., Burlingame, CA). Cells were viewed with an Axioplan epifluorescence microscope (Carl Zeiss, Inc., Thornwood, NY), using either a 40 or 63× oil immersion objective, or a confocal laser scanning microscope (model MultiProbe 2010; Molecular Dynamics, Mountain View, CA). Fluorescent images of stained cells were recorded using Kodak (Rochester, NY) Ektachrome Elite II (ASA 400) film. Photographic images were then digitized with a slide scanner (Nikon, Inc., Melville, NY), and images were resized, arranged, and labeled using Adobe Photoshop software (San Jose, CA). The resulting images were printed from the computer file using a Tektronix dye sublimation printer (Wilsonville, OR). The printed images are representative of the original data.

Cell Extraction, Immunoprecipitation, and Immunoblotting

MDCK cells were grown on Transwell™ filters and extracted in 900 μl Triton X-100 extraction buffer (0.5% [vol/vol] Triton X-100, 10 mM Tris-HCl, pH 7.5, 120 mM NaCl, 25 mM KCl, and 1.8 mM $CaCl_2$) containing 25 mg/ml pepstatin A, 1 mM Pefabloc, 1 mM benzamidine, 1% aprotinin, 100 mM leupeptin, 1 mM sodium vanadate, and 50 mM NaF on a rocker platform for 10 min at 4°C. Cells were scraped from the filter using a rubber policeman and centrifuged at 12,000 *g* for 15 min at 4°C; pellets were dissolved in 100 μl SDS-IP buffer (1% SDS, 10 mM Tris-HCl, pH 7.5, 2 mM EDTA) at 100°C and then diluted with 900 μl Triton X-100 extraction buffer. Supernatants were adjusted with 100 μl SDS-IP buffer for direct separation of proteins for Western blotting or were processed for immunoprecipitation (see below). Protein concentrations in supernatants and pellets were determined using the BCA protein assay reagent kit (Pierce Chemical Co., Rockford, IL). Equal amounts of total protein (reconstituted by addition of supernatant and pellet fraction from each sample), or supernatant or pellet were separated by 7.5% SDS-PAGE, transferred electrophoretically to nitrocellulose filters, and processed for immunoblotting with specific antibodies. Immune complexes were visualized with donkey anti–rabbit and sheep anti–rat horseradish peroxidase–conjugated secondary antibodies (Amersham Corp., Arlington Heights, IL) and developed using the ECL kit (Amersham Corp.). For protein immunoprecipitation, Triton X-100 lysate supernatants were incubated with anti–E-cadherin (Ecad2) antibody, and immune complexes were isolated with protein A–Sepharose (Pharmacia Biotech, Piscataway, NJ). Immunoprecipitates were washed with high stringency buffer (HS-B: 20 mM Tris-HCl, pH 7.5, 120 mM NaCl, 25 mM KCl, 5 mM EDTA, 5 mM EGTA, 0.1% SDS, 1% Na-deoxycholate, 0.5% Triton X-100), followed by high salt wash buffer (HS-B containing 1M NaCl), and samples were then resolved by SDS-PAGE and processed for Western blotting as described above. Chemiluminescent signals were collected and scanned from autoradiography film (Kodak) with a Hewlett-Packard Scan-Jet IIc scanner (Greeley, CO) into Adobe Photoshop. Intensities of signals were measured by NIH Image 1.58 software. For figures, the contrast of images was adjusted, arranged, and labeled in Adobe Photoshop. The resulting images were printed using a Tektronix dye sublimation printer (Wilsonville, OR). The printed images are representative of the original data.

Results

Rac1V12 Induces Lamellipodia Formation and MDCK Cell Scattering, but Rac1N17 Induces Compaction of MDCK Cell Colonies

T23 MDCK cells, which stably express the tetracycline transactivator (Barth et al., 1997), were cotransfected with either NH_2-terminal tagged myc-RhoAV14 (constitutively active RhoA mutant), -RhoAN19 (dominant-negative RhoA mutant), -Rac1V12 (constitutively active Rac1 mutant), or -Rac1N17 (dominant-negative Rac1 mutant) and pHMR272 (hygromycin B resistance). Four clones expressing RhoAV14, five clones expressing RhoAN19, three clones expressing Rac1V12, and four clones expressing Rac1N17 were isolated. Expression of each RhoA or Rac1 mutant was confirmed by immunofluorescence microscopy and Western blotting. Clones were chosen for further analysis based upon the homogeneity and amount of protein expression.

In the first series of experiments, we characterized the cellular effects of (*a*) a gradual increase in amounts of RhoA and Rac1 mutants (Fig. 1); (*b*) long-term expression (3 wk) of Rac1V12 and Rac1N17 (Fig. 2); and (*c*) a DC dose-specified range of fixed amounts of RhoA or Rac1 mutants (Fig. 3). Antibodies that recognized endogenous Rac1 or RhoA were used in Western blots of cell extracts to monitor simultaneously the amounts of mutant and endogenous protein; because of the myc-tag, RhoA and Rac1 mutants had a slower electrophoretic mobility than endogenous RhoA and Rac1. We note that interpretation of observed changes in cellular phenotype is complicated not only by the increasing level of mutant small GTPase, but also by the increasing time that the cells were exposed to mutant protein. Nevertheless, these initial observations provide important, first insights into early changes in epithelial cell organization in response to mutant GTPase expression. Note that this first set of experiments should be compared with those presented in Fig. 3, in which different but constant levels of mutant small GTPases were expressed for the same length of time.

First, cells were grown in DME/FBS and 20 ng/ml DC to repress RhoA or Rac1 mutant expression. Cells were then plated at low cell density in the absence of DC, the accumulation of each RhoA or Rac1 mutant was monitored in Western blots, and the effects of mutant expression on cell morphology were examined by phase contrast microscopy (Fig. 1, *A* and *B*). In the presence of 20 ng/ml DC (0 h), Rac1V12 was not expressed, and cells formed small colonies of adherent cells with few membrane ruffles or lamellipodia, similar to normal MDCK cells (Fig. 1 *A*). After removal of DC, the amount of Rac1V12 accumulated from 10% (12 h), to 40% (24 h), 85% (36 h), and finally 95% (48–60 h) of the level of endogenous Rac1. Note that during this time, the amount of endogenous Rac1 remained approximately constant (Fig. 1 *A*). During the accumulation of Rac1V12, the morphology of cells and colonies

changed. The first effects were apparent at 24 h as cells formed prominent lamellipodia and appeared to have spread out more on the substratum. These changes became more pronounced at later times. At 60 h, colonies of cells were still intact, but the cells were flat with prominent, broad lamellipodia at cell surfaces not in contact with other cells (Fig. 1 *A*; note that the magnification is greater than in the other images).

The kinetics of Rac1N17 accumulation and the effects on cell morphology were different from those of Rac1V12. Initially, Rac1N17 accumulated to ~20% of endogenous Rac1 protein level 12 h after removal of DC, but then the amount increased quickly to ~220% (24 h), ~350% (36 h), and finally >600% of endogenous Rac1 (Fig. 1 *A*). The amount of endogenous Rac1 remained constant for 60 h and then decreased by ~60%. Cellular effects were detected after 24 h as cells became less spread on the substratum and rounded-up, and colonies became increasingly compacted.

A similar analysis of the effects of RhoA mutant accumulation on cell morphology is shown in Fig. 1 *B*. After 12 h, the level of RhoAV14 was not above background (Fig. 1 *B*). RhoAV14 accumulated to 10% (24 h), 70% (36 h), 100% (48 h), and finally 150% (60 h) of endogenous RhoA. The amount of endogenous RhoA remained constant, but finally decreased by ~25% at 60 h (Fig. 1 *B*). During this time, cells remained associated in colonies, but membrane ruffles and lamellipodia at colony edges became more frequent, and translucent gaps formed between cells within colonies (Fig. 1 *B*).

RhoAN19 accumulated slowly in cells and the maximum level of expression relative to the endogenous RhoA level

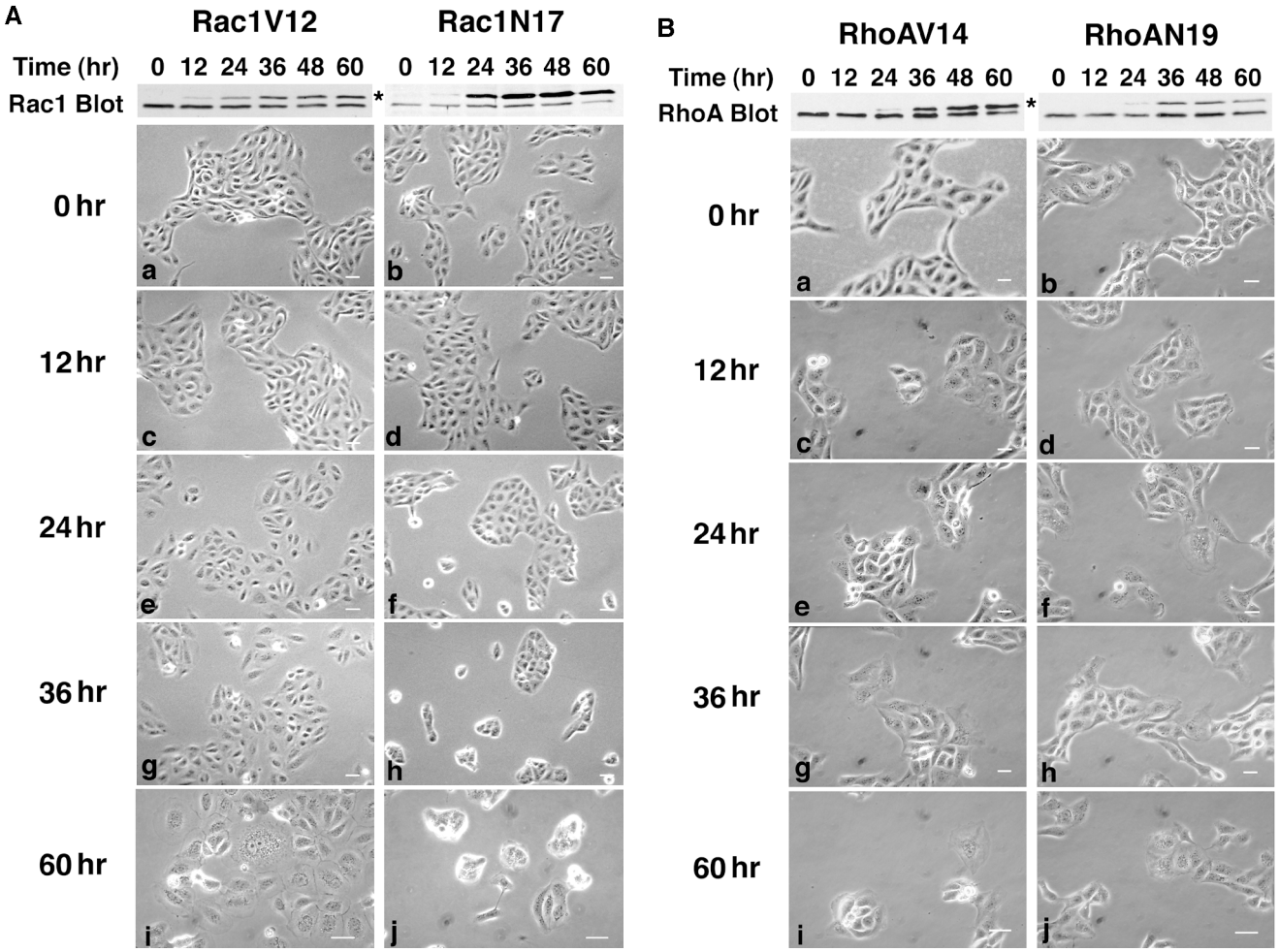

Figure 1. (*A*) Time course of Rac1V12 and Rac1N17 expression in MDCK cells and effects on the cell morphology in low-density cultures. Low-density cultures of Rac1V12 (*left*) and Rac1N17 (*right*) MDCK cells were grown in the absence of DC for the indicated times. (*Top*) At each time, cells were lysed in SDS sample buffer and processed for Western blotting with an anti-Rac1 monoclonal antibody to detect induction of mutant protein and levels of endogenous protein. *Note that addition of the myc epitope tag to Rac1V12 and Rac1N17 caused them to migrate more slowly than endogenous Rac1. (*Bottom*) Phase contrast micrographs of cell colonies at different times after Rac1V12 or Rac1N17 induction. (*B*) Time course of RhoAV14 and RhoAN19 expression in MDCK cells and effects on the cell morphology in low-density cultures. Low-density cultures of RhoAV14 (*left*) and RhoAN19 (*right*) MDCK cells were grown in the absence of DC for the indicated times. (*Top*) At each time, cells were lysed in SDS sample buffer and processed for Western blotting with an anti-RhoA monoclonal antibody to detect induction of mutant protein and levels of endogenous protein. *Note that addition of the myc epitope tag to RhoAV14 and RhoAN19 caused them to migrate more slowly than endogenous RhoA. (*Bottom*) Phase contrast micrographs of cell colonies at different times after RhoAV14 or RhoAN19 induction. Bars, 10 μm.

was lower than that of other RhoA and Rac1 mutants. RhoAN19 was detected at ~15% (24 h), 60% (36–48 h), and finally 45% (60 h) of endogenous RhoA (Fig. 1 *B*). The amount of endogenous RhoA increased by ~25%. During expression of RhoAN19, cells became more spread on the substratum, ruffled membrane and lamellipodia were detected, and cell colonies became less circular and more elongated and fibroblastic in overall shape (Fig. 1 *B*).

Effects of Prolonged Overexpression of Rac1 Mutants in MDCK Cells

Recent studies of RhoA mutants in epithelial cells have used constitutive expression vectors driven by a viral promoter (Takaishi et al., 1997). For comparison, we examined effects of long-term expression of Rac1V12 and Rac1N17 in cells grown in the absence of DC for up to 3 wk. Rac1V12 accumulated to a level similar to that of endogenous Rac1 after 36 h (Fig. 2; see also Fig. 1 *A*) and then remained at that level for 3 wk (Fig. 2). Rac1V12 cell morphology was different from that of control cells grown in the presence of DC to repress Rac1V12 expression. Rac1V12 cells remained in colonies, but the cells were flattened onto the substratum and had abundant lamellipodia; <5% of cells formed compact colonies similar to control (data not shown). The morphology of Rac1V12 cells at 3 wk was similar to the cell morphology after 36 h (see Fig. 1 *A*), indicating that short- and long-term expression of this mutant had similar effects.

Rac1N17 accumulated to >400% of the amount of endogenous Rac1 after 36 h (Fig. 2), as reported above (see Fig. 1 *A*), but then decreased to background levels after 1 wk (Fig. 2). Rac1N17 cells had a similar morphology whether DC was present or not after 3 wk (Fig. 2). We expect that Rac1N17 high expressing cells were lost from the cell population because either they attached poorly to the substratum (Lee, R., and T.-S. Jou, unpublished result) or Rac1N17 suppressed cell growth (Qiu et al., 1995), which could allow a population of firmly attached, faster growing cells to quickly dominate the culture. These results further underline the usefulness of tetracycline repressible gene expression for these studies.

Subcellular Distributions and Dose-dependent Effects of Rac1 and RhoA Mutants on the Actin Cytoskeleton in MDCK Cells

The results described above show that the gradual accumulation of RhoA and Rac1 mutants led to concomitant, mutant protein concentration-dependent changes in cellular morphology. In the next series of experiments, we examined the effects of fixed amounts of RhoA or Rac1 mutants on cell morphology, the subcellular distribution of RhoA and Rac1 mutants, and the organization of F-actin. In these experiments, amounts of RhoA and Rac1 mutants were titrated by growing cells in different concentrations of DC. Relative amounts of mutant and endogenous RhoA or Rac1 were determined by Western blotting with antibodies that recognized Rac1 or RhoA, and the distribution of each RhoA or Rac1 mutant protein was determined with an antibody that recognized the myc epitope tag (Fig. 3, *A–D*).

Levels of Rac1V12 increased from 20% in 20 pg/ml DC, to ~45% in 4.0–0.8 pg/ml DC, to 100% −DC compared with endogenous Rac1. Levels of endogenous Rac1 did not change (Fig. 3 *A*). Rac1V12 protein was first detected (20 pg/ml DC) at cell–cell contacts and continued to accumulate there even when the amount of Rac1V12 had increased 5× higher (−DC). Significantly less protein was detected on the membrane in areas not in contact with other cells (Fig. 3 *A*). Generally, cells appeared more flattened on the substratum in the presence of increasing amounts of Rac1V12, as described above (Fig. 1 *A*). We detected clear changes in F-actin organization as the Rac1V12 level increased. Initially, in the absence of Rac1V12 expression (20 ng/ml DC), F-actin was prominently localized in stress fibers at the base of cells and in thick cortical bundles at the edge of cells (Fig. 3 *A*). With increasing amounts of Rac1V12, F-actin was no longer clearly organized into stress fibers, and thick cortical bundles of actin were sharper in profile and lined up next to cell–cell contacts (Fig. 3 *A*).

Rac1N17 accumulated to levels 10–20 times that of endogenous Rac1 at all DC concentrations below 20 pg/ml. Note that at the same time, levels of endogenous Rac1 de-

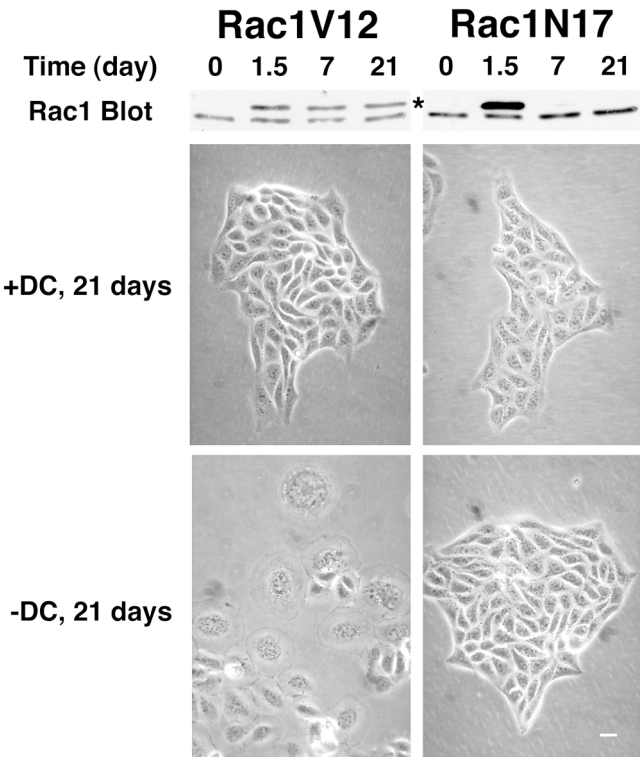

Figure 2. Effects of long-term expression of Rac1V12 and Rac1N17 on mutant protein expression and MDCK cell morphology. Rac1V12 and Rac1N17 MDCK cells were cultured in the presence of DC, 0 d, or in absence of DC for 1.5, 7, or 21 d. (*Top*) At each time, cell lysates were analyzed by Western blotting with an anti-Rac1 antibody to assess the expression of Rac1V12 or Rac1N17, and endogenous Rac1. *Note that addition of the myc epitope tag to Rac1V12 and Rac1N17 caused these proteins to migrate more slowly than endogenous Rac1. (*Bottom*) Phase contrast micrographs of Rac1V12 and Rac1N17 cells grown in the presence (+DC) or absence of DC (−DC) for 21 d. Bar, 10 μm.

creased by ~50% (Fig. 3 *B*). Cells became smaller in profile and colonies became tightly compacted (Fig. 3 *B*), as described above (see Fig. 1 *A*). Rac1N17 localized to cell–cell contacts, and little or no protein accumulated at the edges of cells not in contact with other cells. Some increased diffuse staining of Rac1N17 was also detected in the cytoplasm. The instant high levels of Rac1N17 in 20 pg/ml DC caused F-actin to become localized to cell–cell contacts. However, because of the highly compacted organization of colonies, it was difficult to determine if other aspects of F-actin organization had changed (see below).

RhoAV14 began to accumulate to 5% of endogenous RhoA at 200 pg/ml DC, to ~30% in 0.8 pg/ml DC, to 50% in 20 pg/ml DC, to 180% in 4 pg/ml DC, and to >200% in 0.8 pg/ml DC (Fig. 3 *C*). RhoAV14 was localized in the cytoplasm, was excluded from the nucleus, and did not appear to accumulate at cell–cell contacts (Fig. 3 *C*). With increasing amounts of RhoAV14, F-actin bundles at the base of the cell and at the cell cortex appeared to become thicker and more prominent.

RhoAN19 was detected at concentrations of DC below 20 pg/ml and accumulated to 20% of endogenous RhoA in 20 pg/ml, to 60% in 4 pg/ml, and to 140% in 0.8 pg/ml (Fig. 3 *D*). We detected an ~50% decrease in the amount of endogenous RhoA when RhoAN19 was expressed at maximal level (Fig. 3 *D*). RhoAN19 was localized to the cytoplasm and did not accumulate at cell–cell contacts (Fig. 3 *D*). Despite high levels of RhoAN19, we detected few gross changes in the organization of F-actin, which remained localized in stress fibers and cortical bundles at the edges of cells (Fig. 3 *D*).

Effects of Rac1 and RhoA Mutants on Cellular Morphology and F-Actin Organization in Confluent Monolayers of Polarized MDCK Cells

We next examined the effects of RhoA and Rac1 mutants on cellular organization and F-actin distributions in confluent monolayers of MDCK cells. 18 h after induction of cell–cell contacts, a monolayer that formed in the presence

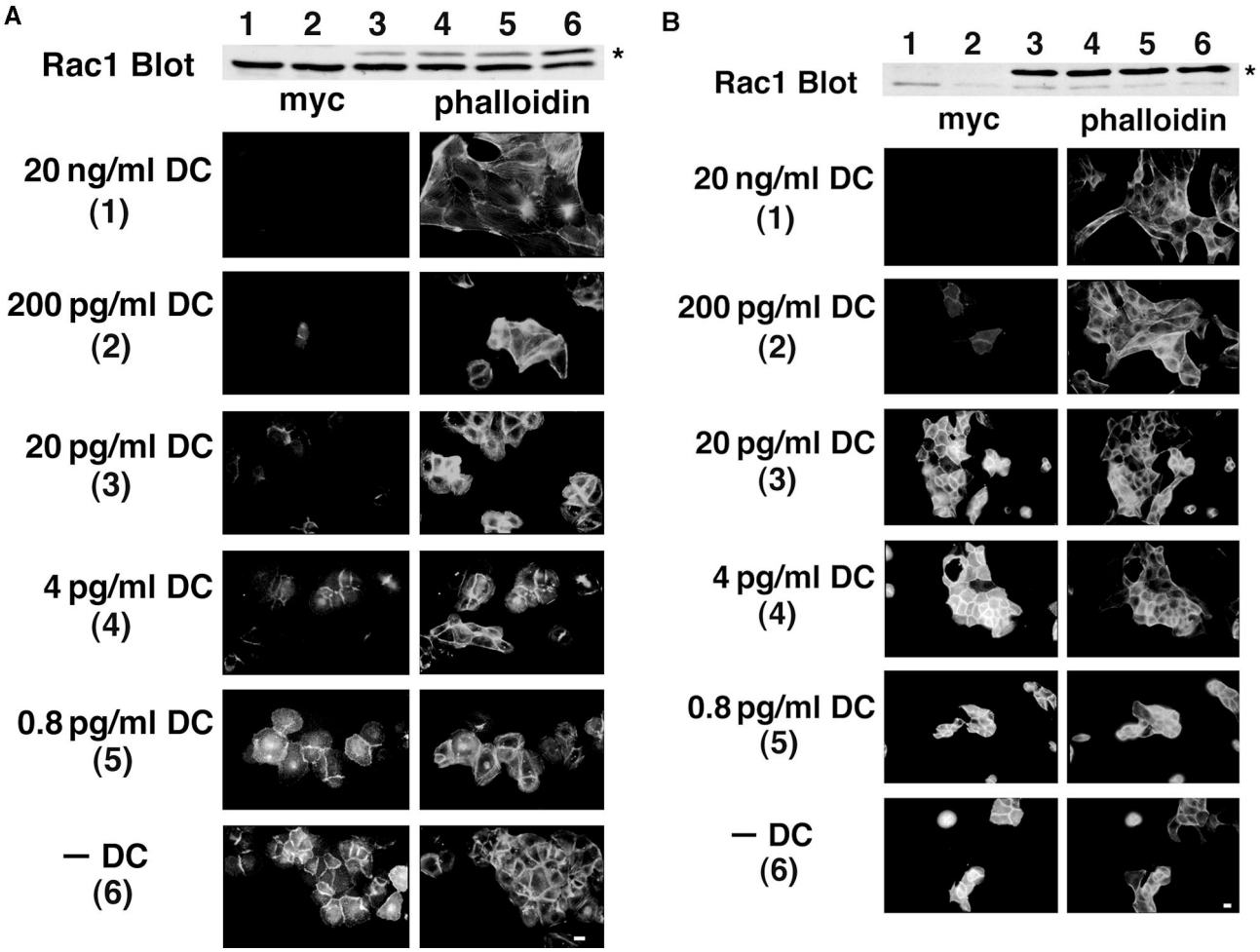

Figure 3. Dose-dependent effects of Rac1V12 (*A*), Rac1N17 (*B*), RhoAV14 (*C*), and RhoAN19 (*D*) on the subcellular distributions of mutant protein (myc-tagged), F-actin distribution (phalloidin), and cell morphology. Low-density MDCK cells were grown for 40 h in the presence of different concentrations of DC. (*Top*) After 40 h, cell lysates were analyzed by Western blotting with a mouse anti-Rac1 or RhoA antibody to assess the expression of mutant protein (*) and endogenous protein. The number above each lane refers to the concentration of DC shown on the left hand side. (*Bottom*) After 40 h, cells were fixed and double stained with a mouse anti-myc antibody to detect mutant RhoA or Rac1, and phalloidin to detect F-actin. Bar, 10 μm.

of DC contained cells that were organized into a regular, cobble-stone pattern (Fig. 4, RhoAV14+DC). Confocal microscopy of these cells stained with phalloidin showed that F-actin was organized into an intensely staining circumferential belt at the apex of the lateral membrane in the region of the apical junctional complex, down lateral membrane at cell–cell contacts, and in weakly staining stress fibers at the base of cells close to the substratum (Fig. 4, RhoAV14+DC).

RhoAV14-expressing MDCK cells also established a continuous monolayer, but the cells were larger and more fusiform than control cells and were irregularly arranged in the monolayer with clear gaps between cells; groups of cells also grew on top of the monolayer (Fig. 4, RhoAV14−DC). F-actin was prominently localized to cell–cell contacts at the apical surface, but the staining was more diffuse than that in control cells. F-actin staining was particularly strong at the base of cells in the form of stress fibers (Fig. 4, RhoAV14−DC). In contrast, RhoAN19 expressing MDCK cell monolayers appeared similar to the controls, as these cells formed a regular organization and F-actin was strongly localized to cell–cell contacts (Fig. 4, RhoAN19−DC).

Rac1V12-expressing MDCK cells established a monolayer of regularly organized cells similar to the control (Fig. 4, Rac1V12−DC). At the apical surface, however, F-actin was not only organized at cell–cell contacts, as in the control, but also in large aggregates in the plane of the apical membrane. Lower down the lateral membrane and at the base of these cells, F-actin was present mostly at cell–cell contacts. Only a few if any stress fibers were visible (Fig. 4, Rac1V12−DC). Rac1N17-expressing cells formed a monolayer of uniformly normal-shaped cells (Fig. 4, Rac1N17−DC). F-actin was prominently localized to the cell–cell contacts at the apex of the lateral membrane. Further down the lateral membrane and at the base of these cells, the F-actin organization was unusually beaded at cell–cell contacts, and there appeared to be few if any stress fibers.

In summary, in confluent cell monolayers expression of RhoA mutants caused a different set of changes in F-actin organization than did Rac1 mutants. RhoAV14 induced more stress fiber formation, as at low cell density. In contrast, both Rac1V12 and Rac1N17 induced an unusual beaded pattern of F-actin on the lateral membrane, although this type of organization was not obvious in cells grown at a low density. In confluent monolayers, F-actin in Rac1V12 cells was also localized in an unusual beaded pattern at the apical membrane. These changes in F-actin distributions prompted us to examine the distributions of actin-associated apical (GP135) and basal–lateral (E-cadherin) membrane proteins in these cells.

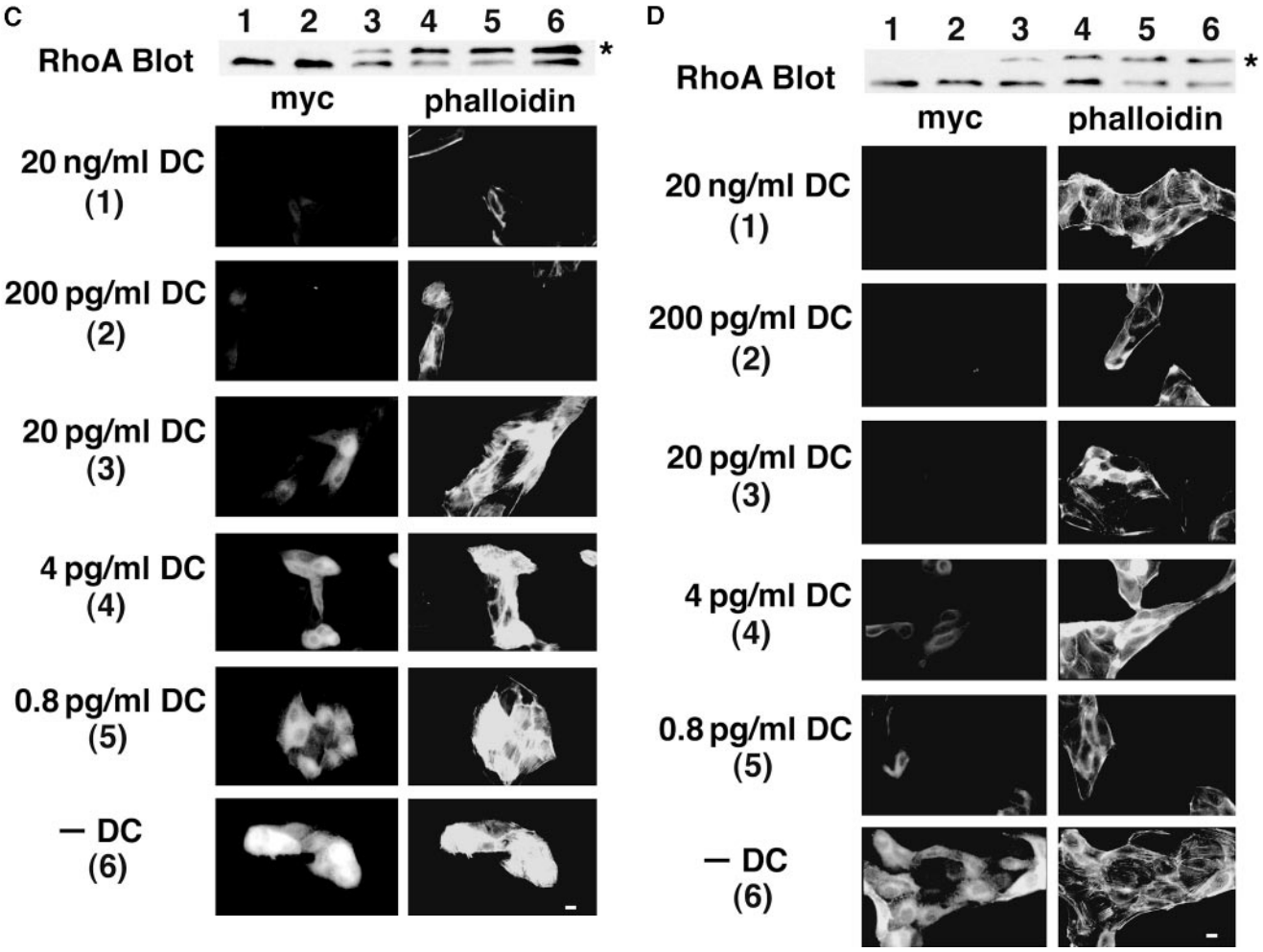

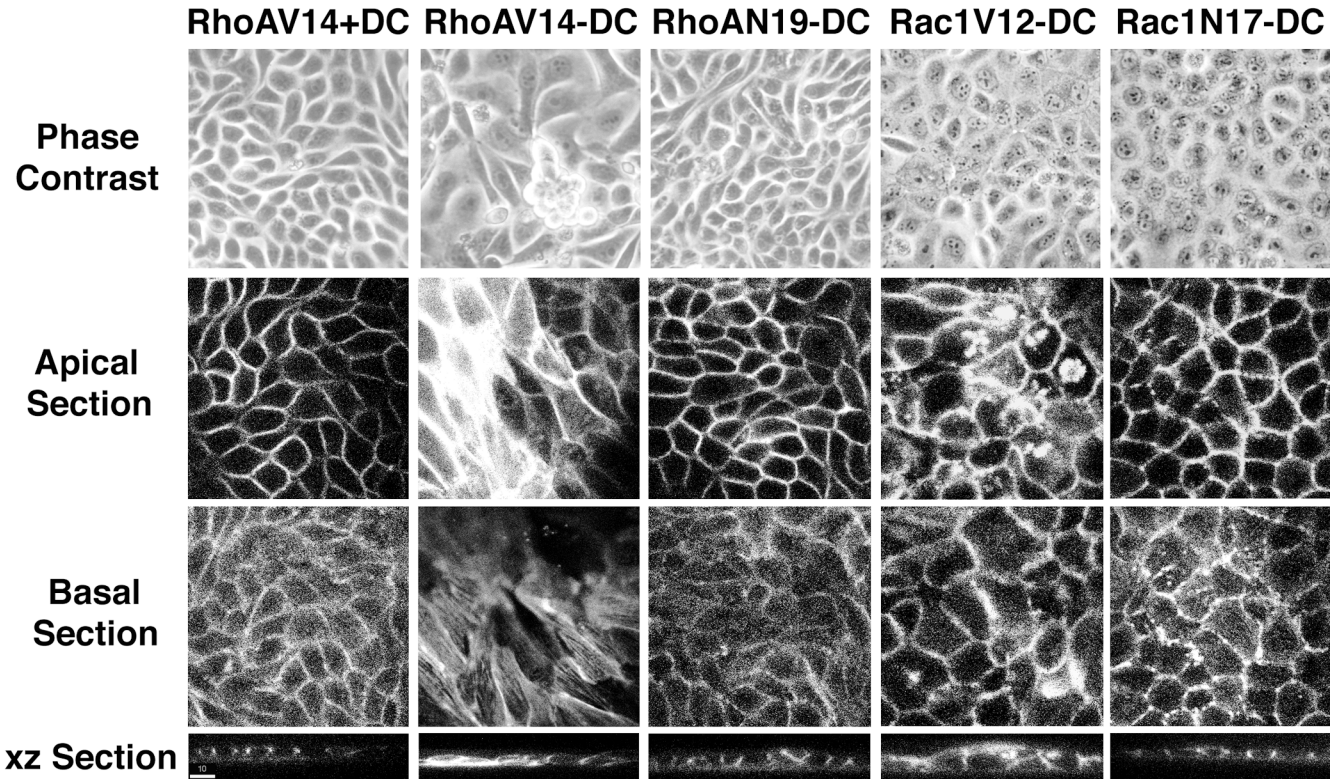

Figure 4. F-actin distribution and morphology of confluent monolayers of control (RhoAV14+DC) and RhoA and Rac1 mutant–expressing MDCK cells (−DC). RhoAV14, RhoAN19, Rac1V12, and Rac1N17 MDCK cells were grown in the presence (control; *first column*) or absence (*all other columns*) of DC at low cell density for 24 h, trypsinized and plated in LCM for 3 h, and then cultured for 16 h in HCM to induce cell–cell adhesion (+/−DC). (*Top*) Phase contrast micrographs of cells. (*Middle*) Cells were fixed and stained with phalloidin and examined by confocal microscopy: *xy* sections at the level of the apical junction (*Apical Section*), and basal membrane (*Basal Section*). (*Bottom*) *xz* sections of cell monolayers. Bar, 10 μm.

Rac1V12 or Rac1N17 Expression Causes Intracellular Aggregation of E-Cadherin/F-Actin and GP135/F-Actin at Different Cell Densities

E-cadherin and GP135 distributions were examined in MDCK cells expressing RhoA or Rac1 mutants at a range of cell densities (Fig. 5). Rac1V12 cells had a flattened morphology at low cell density, as shown above (Fig. 1 *A*). Double fluorescence showed colocalization of Rac1V12 (anti-myc tag antibody) and E-cadherin at the membrane of cell–cell contacts (Fig. 5, *a* and *a′*). Note that both proteins were excluded from regions of the plasma membrane that were not in contact with other cells. As the cell density increased, Rac1V12 remained at cell–cell contacts, but discontinuities in the staining at those contacts were evident (Fig. 5 *b*). At high cell density, Rac1V12 was located in finely beaded arrays at cell–cell contact sites and in large (intracellular) aggregates (Fig. 5 *c′*). These Rac1V12 aggregates colocalized with GP135 (Fig. 5, *c* and *c′*) and with F-actin (see also Fig. 4). Antibodies to extracellular epitopes on GP135 only reacted with these aggregates when cells had been permeabilized with Triton X-100 (data not shown), indicating that the aggregates were intracellular.

Rac1N17 cells were grown at either a low density (Fig. 5, *d* and *f*) or in medium containing 5 μM Ca^{2+} (LCM; see Materials and Methods) to inhibit E-cadherin–mediated cell–cell adhesion (Fig. 5 *e*). At low cell densities, Rac1N17 was localized in large aggregates inside cells that colocalized with F-actin (Fig. 5 *d′*) and E-cadherin (Fig. 5 *e′*), but not GP135 (data not shown). In addition to these aggregates, Rac1N17, E-cadherin, and F-actin also colocalized at cell–cell contacts in finely beaded arrays (Fig. 5, *d–f*). In intermediate-density cultures containing colonies of >15 cells, Rac1N17/E-cadherin aggregates were often enriched at the free margins of cells and diminished greatly in number in cells that were completely surrounded by other cells (Fig. 5, *g* and *g′*). In high-density cultures, intracellular Rac1N17 aggregates were no longer visible (Fig. 5 *h*), and Rac1N17 was localized in a finely beaded pattern at cell–cell contacts, similar to that of F-actin (Fig. 4) and E-cadherin/β-catenin (see Fig. 7 *A*).

In Polarized Cell Monolayers, RhoA and Rac1 Mutants Do Not Affect E-Cadherin/β-Catenin Distribution, but Rac1 Mutants Affect the Localization of GP135

The preceding results show that RhoA and Rac1 mutants affect the distributions of F-actin, E-cadherin, and GP135 during initial stages in the formation of a confluent cell monolayer and the development of epithelial cell polarity. We next examined the organization of E-cadherin and GP135 in confluent monolayers of polarized MDCK cells grown on Transwell™ filters. Steady-state levels of E-cadherin

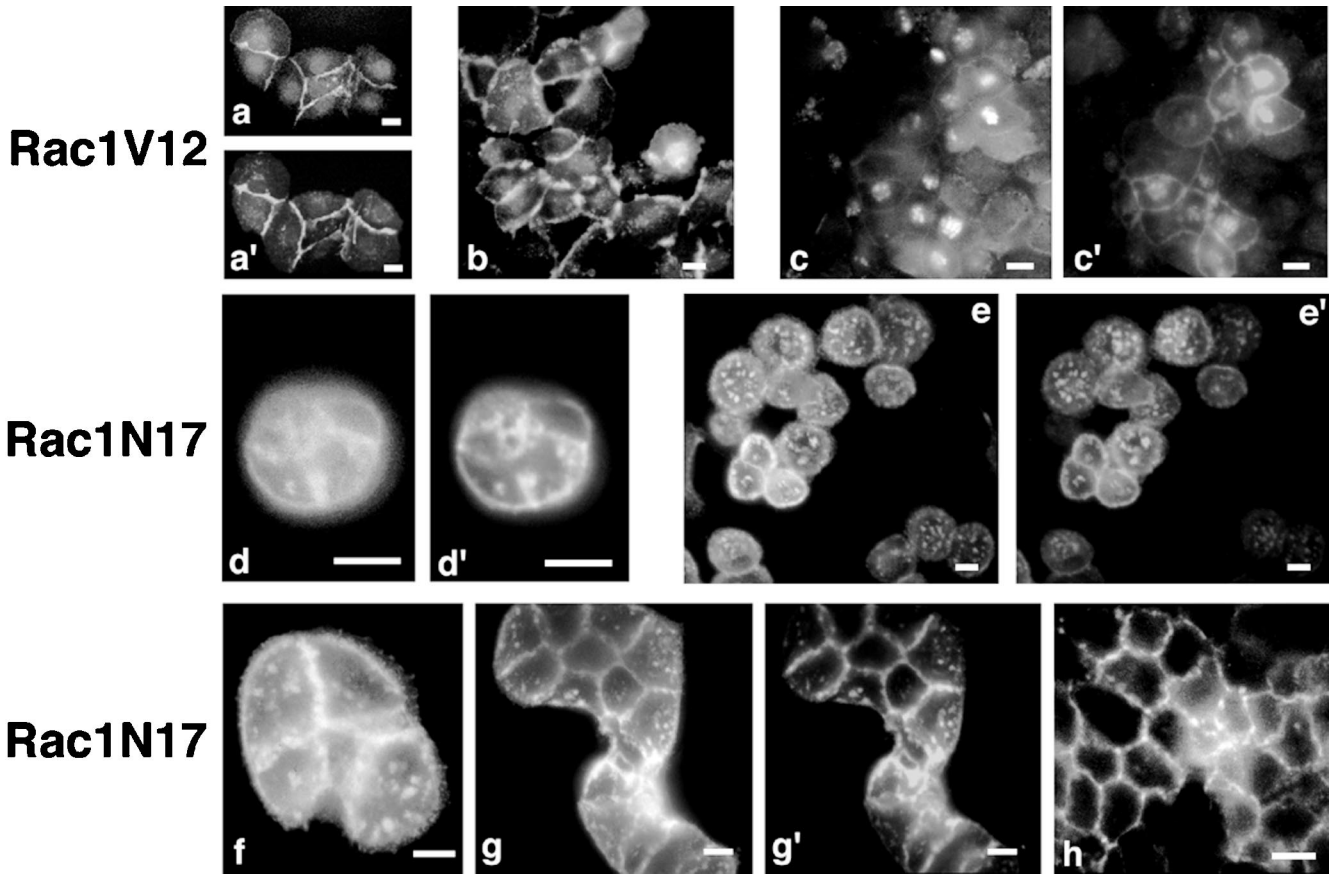

Figure 5. Colocalization of Rac1 mutants with either E-cadherin or GP135, depending on cell density. Rac1V12 and Rac1N17 cells were cultured without DC for 16 h at low (*a*, *a′*, *d*, *d′*, *e*, *e′*, and *f*), intermediate (*b*, *g*, and *g′*), or high cell density (*c*, *c′*, and *h*) in LCM (*e* and *e′*) or HCM (*a*, *a′*, *b*, *c*, *c′*, *d*, *d′*, *f*, *g*, *g′*, and *h*). Cells were fixed and processed for immunofluorescence microscopy with anti-myc (*a*, *b*, *c′*, *d*, *e*, *f*, *g*, and *h*) and either anti–E-cadherin (*a′*, *e′*, and *g′*) or anti-GP135 (*c*) antibodies, or FITC phalloidin (*d′*). Bar, 10 μm.

and the associated cytoplasmic proteins α- and β-catenin were analyzed by Western blotting of E-cadherin–specific coimmunoprecipitates (Fig. 6). Little or no change in levels of any of these proteins was detected between matched pairs of controls (+DC) and RhoA or Rac1 mutant cells (−DC).

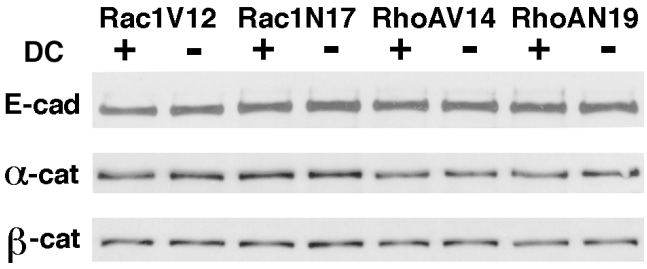

Figure 6. Protein levels of the E-cadherin, β-catenin, and α-catenin complex in cells expressing Rac1 or RhoA mutants. Rac1V12, Rac1N17, RhoAV14, and RhoAN19 MDCK cells were grown on Transwell™ filters for 16 h in the presence (lanes labeled +, control) or absence (lanes labeled −) of DC and then processed for immunoprecipitation with E-cadherin antibody followed by Western blotting of the coimmunoprecipitated complex with antibodies specific for E-cadherin, β-catenin, or α-catenin.

Confocal microscopy showed that E-cadherin and β-catenin were localized to the lateral membrane of control cells (Fig. 7 *A*, RhoAV14+DC) and of all cells expressing RhoA or Rac1 mutants (*−DC*). In all cases, little or no E-cadherin or β-catenin was detected at either the apical or basal membrane (Fig. 7 *A*). However, careful examination of the staining patterns revealed that the distribution of E-cadherin in cells expressing RhoAV14 (−DC), Rac1V12 (−DC), and Rac1N17 (−DC) was different from that in the control (RhoAV14+DC) and RhoAN19−DC cells (Fig. 7 *A*). In RhoAV14 cells, E-cadherin and β-catenin staining were more diffuse at the membrane (Fig. 7 *A*), similar to that of F-actin in these cells (Fig. 4). In Rac1V12 and Rac1N17 cells, E-cadherin and β-catenin staining revealed a finely beaded pattern at cell–cell contacts (Fig. 7 *A*), similar to the distribution of F-actin on the lateral membrane of these cells (Fig. 4).

Fig. 7 *B* shows apical membrane *xy* sections (*left*) and confocal *xz* sections (*right*) of MDCK monolayers stained with antibodies to E-cadherin and GP135. The *xy* sections show that GP135 has a finely granular staining pattern on the apical surface of control cells (RhoAV14+DC), and the *xz* section of these cells shows that GP135 is restricted to the apical surface and excluded from lateral membranes containing E-cadherin, as expected (Ojakian and Schwim-

mer, 1988). In RhoAV14 (−DC) expressing cells, GP135 staining was different from that in control cells. Relatively little GP135 was detected at the apical surface, and the majority of GP135 staining appeared to be either associated with the lateral membrane or in intracellular aggregates. In contrast, GP135 staining in RhoAN19 (−DC) expressing cells appeared very similar to that in control cells. In Rac1V12 (−DC) expressing cells, GP135 staining was

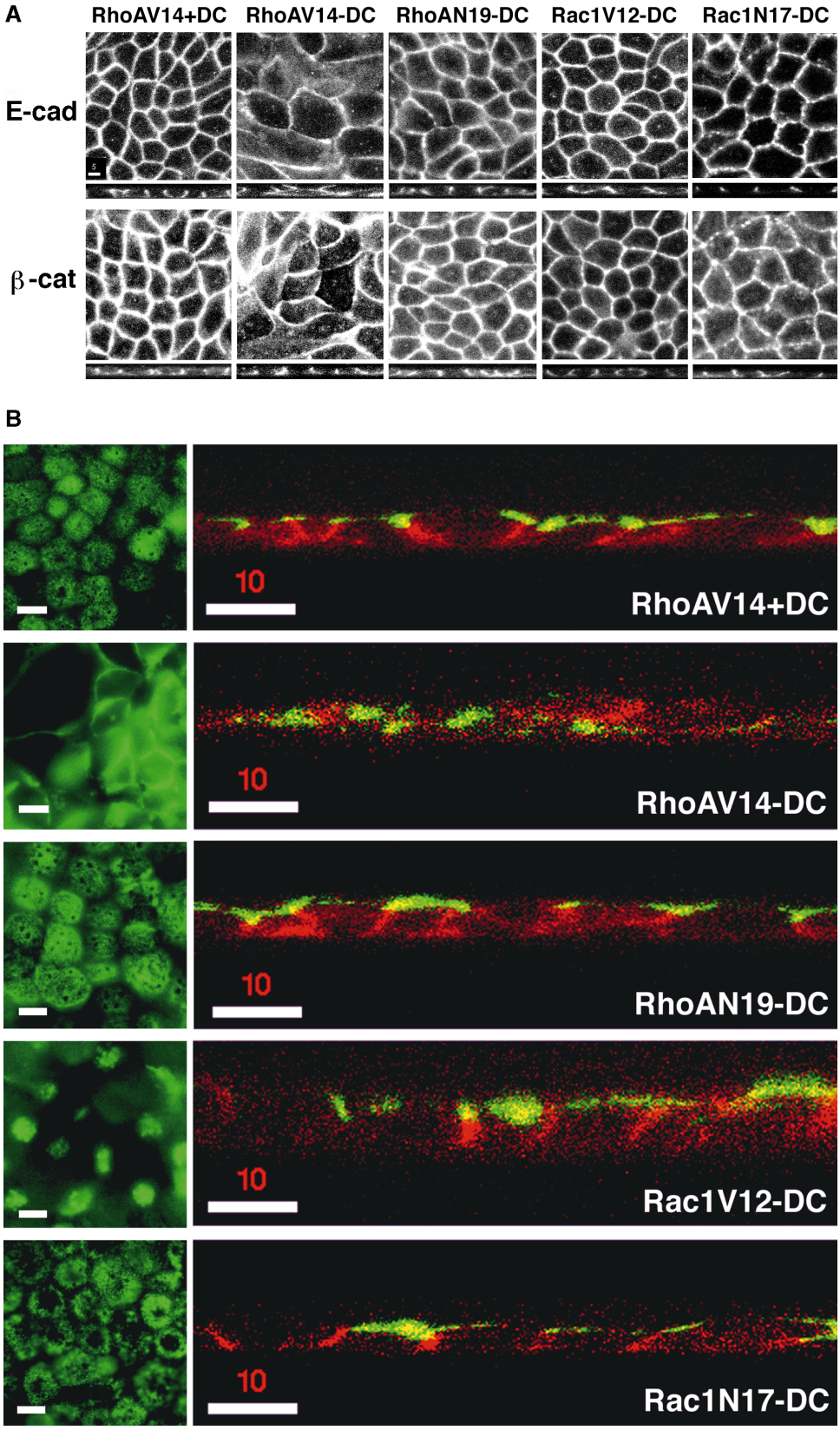

Figure 7. (*A*) Distribution of E-cadherin and β-catenin in confluent monolayers of control (RhoAV14+DC) and RhoAV14 (−DC), RhoAN19 (−DC), Rac1V12 (−DC), and Rac1N17 (−DC) expressing MDCK cells. RhoAV14, RhoAN19, Rac1V12, and Rac1N17 MDCK cells were grown in the presence (control; *left column*) or absence (*all other columns*) of DC at low cell density for 24 h, trypsinized and plated in LCM for 3 h, and then cultured for 16 h in HCM to induce cell–cell adhesion (with or without DC). After fixation, cells were stained with anti–E-cadherin (*top*) and β-catenin (*bottom*) antibodies and then examined in a confocal microscope. *xy* sections (*large panels*), at the level of apical junction, and *xz* sections are shown. (*B*) Distributions of E-cadherin and GP135 in confluent monolayers of control (RhoAV14+DC) and RhoAV14 (−DC), RhoAN19 (−DC), Rac1V12 (−DC), and Rac1N17 (−DC) expressing MDCK cells. RhoAV14, RhoAN19, Rac1V12, and Rac1N17 MDCK cells were grown in the presence or absence of DC at low cell density for 24 h, trypsinized and plated in LCM for 3 h, and then cultured for 16 h in HCM to induce cell–cell adhesion (+/−DC). After fixation, cells were costained with anti–E-cadherin (TRITC, *red*) and anti-GP135 (FITC, *green*) antibodies. *xy* sections (*left*, GP135 only) were collected by epifluorescence microscopy, and *xz* sections (*right*, E-cadherin and GP135) were collected by confocal microscopy. Bars: (*A*) 5 μm; (*B*) 10 μm.

clearly abnormal compared with controls and appeared aggregated near the apical membrane, similar to the organization of F-actin in these cells (Fig. 4). Antibodies to extracellular epitopes on GP135 only reacted with these aggregates when cells had been first permeabilized with Triton X-100 (data not shown), indicating that the aggregates were intracellular. In contrast, in Rac1N17 (−DC) expressing cells, GP135 staining was restricted to the apical membrane as in controls, although the fine granular staining was excluded from the center of the apical membrane.

Fig. 8 shows a comparison of the distributions of GP135, Rac1V12 (myc), F-actin (phalloidin), and rab11, a member of the rab family of small GTPases that regulates vesicle delivery to target membranes (Lazar et al., 1997; Novick and Zerial, 1997). In Rac1V12 cells grown in the presence of DC (+DC), rab11 was diffusely distributed in the cytoplasm, although an occasional bright aggregate of staining was observed. Double immunofluorescence of Rac1V12 cells grown in the absence of DC (−DC) shows that rab 11 and Rac1V12 colocalized in a single, large aggregate localized in the center of each cell. Note that the rab11 staining was no longer diffuse in the cytoplasm of these cells. The intensity of rab11 staining in the central aggregate correlated positively with the intensity of Rac1V12 staining in the higher expressing cells. Fig. 8 also shows that GP135 and F-actin colocalized in the same aggregates.

Mutant RhoA Dominates Rac1 in Controlling Actin Cytoskeleton Organization and Cell Shape in Doubly Transfected MDCK Cells

Microinjection studies in Swiss fibroblasts have revealed that RhoA is downstream of Rac1 in a signaling pathway (Hall, 1998). However, it is still not clear whether the same signaling hierarchy exists in cell types other than fibroblasts. To test this possibility, we transiently transfected RhoAN19 or RhoAV14 tagged with a Glu-Glu epitope into either the Rac1V12- or the Rac1N17-expressing cell line (Fig. 9). In the presence of RhoAN19, Rac1V12 was no longer localized to cell–cell contacts but was present in the cytoplasm. Furthermore, in the presence of RhoAN19 and Rac1V12, actin filaments were less prominent at the cell periphery and more clearly incorporated into stress fibers at the base of the cell, and the cells became slightly more flattened onto the substratum. Both phenotypes were characteristic of RhoAN19 cells (see Fig. 1). Expression of RhoAV14 in Rac1N17-expressing cells also caused the loss of Rac1N17 from cell–cell contacts. The organization of F-actin and the morphology of cells coexpressing

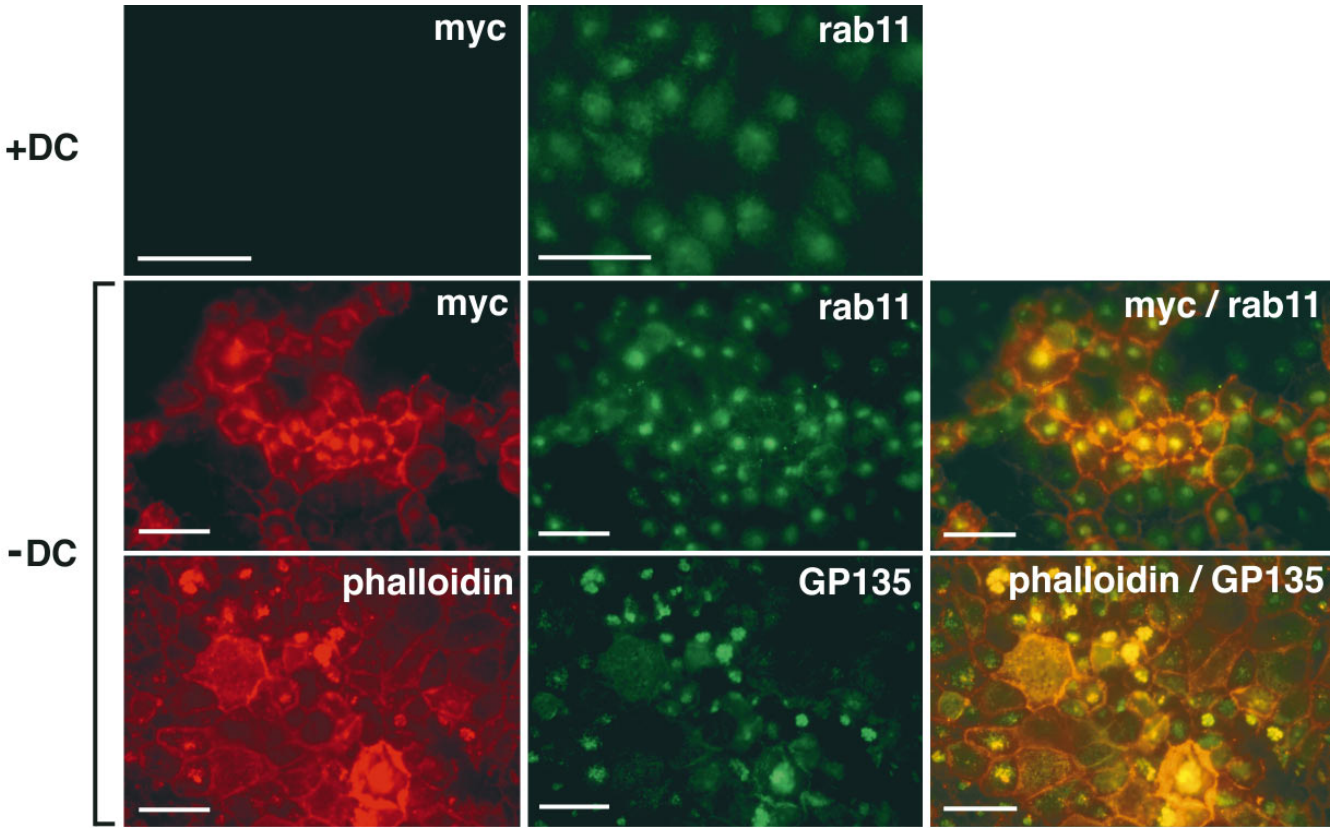

Figure 8. Distributions of rab11, Rac1V12-myc, GP135, and F-actin in monolayers of control cells (Rac1V12 +DC) or Rac1V12 (−DC) expressing MDCK cells. Rac1V12 MDCK cells were grown in the presence (+DC, control) or absence (−DC) of DC at low cell density for 24 h, trypsinized and plated in LCM for 3 h, and then cultured for 16 h in HCM to induce cell–cell adhesion (+/−DC). After fixation, cells were costained with anti-myc (TRITC, *red*) and anti-rab11 (FITC, *green*) antibodies, or TRITC-phalloidin (*red*) and anti-GP135 (FITC, *green*) antibody; double exposures for myc/rab11 and phalloidin/GP135 are shown on the right. *xy* sections were collected by epifluorescence microscopy. Bars, 10 μm.

Rac1N17 and RhoAV14 also resembled those in RhoAV14-expressing cells. Cells doubly expressing Rac1V12 and RhoAV14 exhibited a distribution of F-actin more similar to that in RhoAV14-expressing cells. These data indicate that Rac1 and RhoA are not hierarchically ordered in the same pathway in these cells but act independently on similar targets.

Discussion

Regulated Expression of RhoA and Rac1 Mutants in MDCK Cells

We have characterized cell lines that express RhoA or Rac1 mutants in MDCK cells under control of the tetracycline repressible transactivator. To our knowledge, this series of studies is the first to directly compare amounts of expressed RhoA or Rac1 mutant protein with endogenous RhoA or Rac1 and to compare the effects of a range of known amounts of RhoA or Rac1 mutant proteins on cell structure and function. Although we compared expression levels of mutant RhoA and Rac1 with levels of the equivalent endogenous proteins, the antibodies that recognized endogenous RhoA or Rac1 could not distinguish between the GDP- or GTP-bound forms of these small GTPases. However, we note that a previous analysis of the relative amounts of GDP- and GTP-bound forms of Rac1 in fibroblasts showed that only a very small portion of the total protein was GTP bound in resting cells (Hawkins et al., 1995).

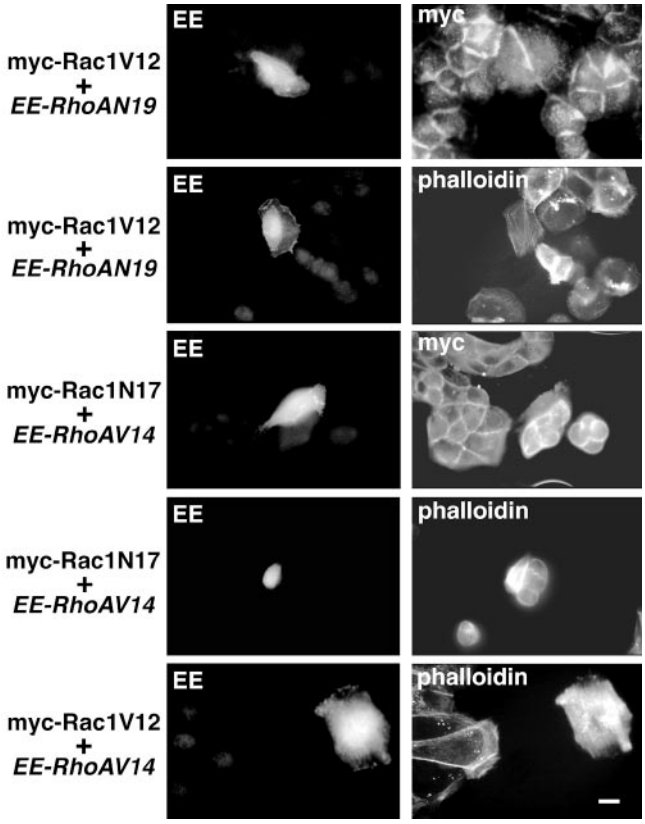

Figure 9. Distribution of RhoA and Rac1 mutants, and F-actin in MDCK cells expressing combinations of Rac1V12, Rac1N17, RhoAV14, and RhoAN19. Rac1V12 (myc) expressing cells were transiently supertransfected with either RhoAN19 tagged with a Glu-Glu epitope (EE) or RhoAV14 tagged with a Glu-Glu epitope (EE). After 24 h, cells were fixed and stained with anti–Glu-Glu epitope tag antibody (EE) to detect cells that expressed RhoAN19 or RhoAV14, and double stained with either myc epitope antibody (myc) or phalloidin to detect Rac1V12 and F-actin, respectively. Rac1N17 (myc) expressing cells were transiently supertransfected with RhoAV14 tagged with a Glu-Glu epitope (EE), stained with antibody recognizing Glu-Glu epitope tag (EE), and double stained with either myc epitope antibody (myc) or phalloidin to detect Rac1N17 and F-actin, respectively. Bar, 10 μm.

The tetracycline repressible system enabled us to tightly regulate levels of RhoA and Rac1 mutant expression. In the presence of more than 20 ng/ml DC, expression of all RhoA and Rac1 mutant genes was fully repressed, and no protein accumulated (Fig. 1, *A* and *B*), thereby providing an important control for these studies. At DC concentrations below 20 ng/ml, Rac1V12, Rac1N17, and RhoAV14 accumulated gradually to levels similar to, or greater than those of endogenous RhoA or Rac1. In the case of RhoAN19, protein levels did not increase above 60% of endogenous RhoA (Fig. 1, *A* and *B*). During the accumulation of RhoA or Rac1 mutant protein, amounts of endogenous RhoA or Rac1 remained constant for ~48 h, until maximum levels of mutant protein were expressed. After 60 h, amounts of endogenous Rac1 decreased by ~60% in the presence of Rac1N17, and RhoA decreased by ~25% or increased by ~25% in the presence of RhoAV14 and RhoAN19, respectively. At present, we do not understand how or why endogenous RhoA and Rac1 levels changed under these conditions. It is possible that transcriptional or posttranslational regulation of endogenous RhoA and Rac1 levels is sensitive to the total amount of RhoA or Rac1 in the cell, or the availability of targets or regulators (e.g., GAP, GEF).

We found that amounts of RhoA or Rac1 mutants well below those of endogenous RhoA or Rac1 disrupted cell structure and organization. Cellular changes were observed with amounts of Rac1V12, RhoAV14, and RhoAN19 that were 40, 10, and 15%, respectively, of endogenous Rac1 or RhoA. We did not determine a "minimal" expression level of Rac1N17 that affected cellular organization since its level increased sharply to >200% of endogenous Rac1 at DC concentrations below 20 ng/ml (Fig. 1 *A*).

How can substoichiometric amounts of RhoA or Rac1 mutants compete with endogenous RhoA and Rac1 to cause changes in cellular organization? One possibility is that RhoA or Rac1 mutants simply bind to available targets, regulators or effectors that are in excess of the amount of endogenous RhoA or Rac1. In this case, the effects of an initially small amount of mutant GTPase would be diluted by the surrounding population of active GTPase. Alternatively, or in addition, RhoA or Rac1 mutants bind to sites made available by the rapid cycling of endogenous RhoA or Rac1 on and off that binding site and then remain there, because dissociation from that site is inhibited by the mutation, thereby blocking the rebinding of endogenous RhoA or Rac1. In this case, mutant GTPases would rapidly displace normal GTPase from binding sites and accumulate, thereby resulting in quick domination of the mutant phenotype. There is indirect evidence in sup-

port of the second possibility: (*a*) RhoA GTPases quickly cycle between active (GTP-bound) and inactive (GDP-bound) states (Bourne, 1993); (*b*) Tiam-1, a nucleotide exchange factor for RhoA GTPases, is localized to cell–cell contacts in MDCK cells (Hordijk et al., 1997); and (*c*) recovery of normal functions after repression of RhoA or Rac1 mutant expression is delayed by ~12 h, indicating that mutant proteins can block activities of endogenous RhoA or Rac1 for long periods (Jou et al., 1998).

An important question is whether Rac1 and RhoA share downstream effectors. We note that both Rac1V12 and Rac1N17 were localized prominently to cell–cell contacts, whereas RhoAV14 and RhoAN19 were located in the cytoplasm (see also Takaishi et al., 1997). Despite these different distributions, we found that coexpression of RhoAN19 in a Rac1V12 background or RhoAV14 in either a Rac1V12 or Rac1N17 background caused delocalization of Rac1 mutants to the cytoplasm and resulted in cell flattening on the substratum and formation of prominent actin stress fibers, both of which are characteristics of RhoAN19 and RhoAV14 cells. These results could be interpreted as showing that active RhoA is required for Rac1 function, similar to that drawn from the study of keratinocytes comicroinjected with C3 transferase and an activated form of Rac1 (Braga et al., 1997). However, we were also able to ask this question in a different way by coexpressing RhoAV14 in a Rac1V12 background. If active RhoA is required for Rac1 function, we would expect a Rac1V12 phenotype of the double transfectant. The results showed that the cellular phenotype of double transfectants was that of RhoAV14 cells. The simplest explanation of our results is that RhoA-induced changes in cellular organization dominate changes induced by Rac1, including the displacement of Rac1 from binding sites at cell–cell contacts. At present, we do not understand the mechanism(s) involved. That RhoA displaces Rac1 directly seems unlikely since the distributions of these proteins are grossly different. Alternatively, RhoA may induce a change in cellular structure/organization that effects Rac1 activity/distribution resulting in displacement of Rac1 (see below).

RhoA and Rac1 Regulate the Organization of Distinct Actin Cytoskeletons Associated with Basal, Lateral, and Apical Membrane Domains

Targets of RhoA and Rac1 activity in fibroblasts are associated with actin membrane structures characteristic of single, motile cells, including stress fibers and focal adhesions (RhoA), and lamellipodia and membrane ruffles (Rac1) (Burridge et al., 1997; Hall, 1998). Note that at low cell densities, the effects of RhoA and Rac1 mutants on MDCK cells were similar to those induced in fibroblasts (Ridley and Hall, 1992; Ridley et al., 1992), including increased formation of stress fibers and cell spreading (RhoA), and increased lamellipodia and ruffled edges (Rac1). These results indicate that the targets of RhoA and Rac1 in fibroblasts and epithelial cells may be similar when epithelial cells are single, motile, and nonpolarized. In contrast to fibroblasts, however, polarized epithelial cells assemble different types of actin structures in association with structurally and functionally distinct basal, lateral, and apical plasma membrane domains. These actin structures are (*a*) stress fibers at the basal surface next to the substratum (Burridge et al., 1997), (*b*) a circumferential organization of actin filaments at lateral membranes in association with cell–cell junctional complexes (Takeichi, 1991), and (*c*) actin bundles and a terminal web associated with microvilli at the apical membrane (Mooseker, 1985). Changes in actin organizations in polarized cells and the ensuing effects of cellular organization were dependent on which RhoA or Rac1 mutant was expressed.

F-actin staining was significantly more intense and had an unusual beaded organization (rather than the continuous line in control cells) at cell–cell contacts of both Rac1V12 and Rac1N17 cells. Takaishi et al. (1997) reported that F-actin staining was weaker at cell–cell contacts of MDCK cells expressing Rac1N17, but strong in Rac1V12 cells as we showed here. The different Rac1N17 result might be due to the wide difference in levels of expression between the studies. In our study, expression levels of Rac1V12 and Rac1N17 were equal to or higher than endogenous Rac1 by Western blotting of whole cell extracts, whereas they were not detectable in the study by Takaishi et al. (1997). We do not know why the distribution of F-actin was more beaded than linear. It is possible that this organization reflected an increase in recruitment and assembly of F-actin at those sites, and/or changes in lateral membrane structure such as increased interdigitations (Takaishi et al., 1997). The actin organization was also different at the apical membrane domain of both Rac1V12 and Rac1N17 cells compared with controls. In general, we detected weaker staining of F-actin in stress fibers in cells expressing Rac1V12 or Rac1N17 than in controls. In RhoAV14 and RhoAN19 cells, F-actin was prominently localized in stress fibers at the base of cells and in a broad cortical belt at lateral membranes that contrasted with the finely beaded distribution in cells expressing Rac1 mutants. In general, the RhoAV14 and RhoAN19 cells spread flatter on the substratum and became more fibroblastic in morphology, but cell–cell contacts were maintained.

As epithelial cells transform from single, motile cells to a static monolayer of polarized cells, the organization of actin changes from one that functions in cell–substratum adhesion and motility to one that also maintains cell–cell adhesion and protein distributions at lateral and apical membrane domains. RhoA may regulate actin structures that determine cell–substratum contact and motility in single cells, as in fibroblasts (Ridley and Hall, 1992; Ridley et al., 1992), whereas Rac1, and possibly RhoA, may regulate actin structures associated with cell–cell contacts and specialization of the apical membrane in cell monolayers. Note that in double transfectants, the fibroblastic phenotype of RhoA mutants dominated the Rac1 phenotype, indicating that the ground state for these cells may be a motile, fibroblastic morphology and that combinatorial effects of RhoA and Rac1 help to drive these cells towards an epithelial phenotype. We do not know how changes in actin organizations between cell–substratum contacts, cell–cell contacts, and the apical membrane might be orchestrated by Rac1 or RhoA. We also do not know if addition of actin to one structure (e.g., cell–cell contacts) is made at the expense of actin in another structure (e.g., cell–sub-

stratum contacts). In this context, it is interesting to note that Friederich et al. (1989) showed that expression of villin induced growth of actin-containing microvilli from the free surface of fibroblasts and, concomitantly, a decrease in the density of stress fibers at the base of the cell.

Recent studies have identified some targets for RhoA GTPases that precipitate changes in the actin cytoskeleton. Rho-kinase is a potentially important target as its activity affects many regulators of the actin cytoskeleton, including myosin II, ERM proteins (Burridge et al., 1997), and adducin (Kimura et al., 1998). Another target may be phosphatidylinositol 4-phosphate 5-kinase (Chong et al., 1994), which regulates PIP_2 synthesis. PIP_2 has broad effects on the actin cytoskeleton by binding to actin-monomer binding proteins (e.g., profilin), which results in release of actin monomers (Lassing and Lindberg, 1985; Goldschmidt et al., 1990). As these targets were identified in single, motile cells, it is possible that they are important at least in actin organization at cell–substratum contacts in single nonpolarized cells and in polarized epithelial cells. Whether they are important in actin organizations at cell–cell contacts or actin membrane specializations in these cells will need further study. We note, however, that the ERM family (radixin, Matsui et al., 1998; ezrin, Chen et al., 1995; Yao and Forte, 1996) and adducin (Kaiser et al., 1989) have been implicated in the organization of cell–cell adhesion and the actin cytoskeleton.

Different Effects of RhoA and Rac1 Mutants on the Distribution of Apical and Basal–Lateral Membrane Proteins

We showed that changes in F-actin induced by expression of RhoA or Rac1 mutants also correlated with compensatory changes in the distribution and organization of two actin-associated proteins, E-cadherin and GP135. Interestingly, the effects of Rac1 mutants depended on the stage of development of cell polarity. At low density, when cells had just initiated cell–cell contacts, Rac1V12 and E-cadherin colocalized at cell–cell contacts in a linear staining pattern similar to that of E-cadherin in controls. Braga et al. (1997) observed a similar increase in cadherin staining during formation of cell–cell contacts in keratinocytes. Although Rac1N17 and E-cadherin also colocalized at cell–cell contacts, we found both proteins in large aggregates that were not associated with cell–cell contacts. Similar observations were not reported by Takaishi et al. (1997), but they did not examine low-density cultures. We have preliminary evidence that E-cadherin is recruited from intracellular stores to cell–cell contacts during initial stages of cell–cell adhesion (Siemers, K., and W.J. Nelson, unpublished results), and it is possible that Rac1N17 somehow inhibits the release of E-cadherin from these stores, perhaps by affecting linkage of E-cadherin and the actin cytoskeleton, which is critical for the maturation of cell–cell contacts (Adams, C., Y.-T. Chen, S. J Smith, and W.J. Nelson, manuscript submitted for publication). Nevertheless, the sequestration of E-cadherin in membranes not at cell–cell contacts would decrease the amount of E-cadherin available for cell–cell adhesion. Braga et al. (1997) reported that microinjection of Rac1N17 into keratinocytes during induction of cell–cell adhesion caused cadherin to disappear from cell–cell contacts, although it was not clear if E-cadherin was degraded or redistributed. However, our study, and that of Takaishi et al. (1997) demonstrated that steady-state amounts of E-cadherin and catenins in cells expressing RhoA or Rac1 mutants were similar to those in controls, indicating that changes in E-cadherin organization were likely due to protein redistribution rather than degradation.

In polarized cell monolayers at confluent cell density, we observed that in Rac1V12 cells, E-cadherin and F-actin had a finely beaded organization at cell–cell contacts that appeared denser than in controls. This confirms results of recent studies of Rac1V12 expression in MDCK cells (Takaishi et al., 1997) and Rac1L61 expression in keratinocytes (Braga et al., 1997). However in contrast to those studies, we found that E-cadherin and F-actin were still localized to cell–cell contacts in the presence of Rac1N17. Takaishi et al. (1997) reported decreased staining intensity of E-cadherin/catenins at MDCK cell–cell contacts, although protein levels were the same as in the control, and Braga et al. (1997) reported loss of E-cadherin from keratinocyte cell–cell contacts when Rac1N17 was microinjected 3 h after induction of cell–cell adhesion. We note that levels of Rac1N17 expression in our studies were more than sixfold higher than the endogenous Rac1 level, whereas in studies by Takaishi et al. (1997) the amount of Rac1N17 expressed was too low to be detected in Western blots of whole cell lysates. In the study by Braga et al. (1997), effects of Rac1N17 were reported in cells that had just formed cell–cell contacts, with results similar to those reported here (see above), but were not reported in established cell monolayers. That Rac1N17 had a different effect on E-cadherin/actin organization in confluent MDCK cell monolayers is also indicated by the observation that intracellular aggregates containing Rac1N17, E-cadherin, and F-actin, which were prominent in small colonies of cells, were not found in polarized cell monolayers. It is possible that long-term cell–cell contacts are more refractory to the effects of Rac1N17, perhaps as a result of the reorganization of actin after the establishment of cell–cell contacts (see above).

We also examined the distribution of an apical membrane protein, GP135, in cells expressing different RhoA or Rac1 mutants. We found that expression of RhoA and Rac1 mutants had little effect on GP135 organization at low cell densities. However, in confluent monolayers GP135 distribution was disrupted in cells expressing Rac1 or RhoA mutants: in Rac1V12 cells, GP135 was tightly clumped beneath the apical membrane; in Rac1N17 cells, the distribution of GP135 was similar to the control, but the fine, granular staining appeared to be excluded from the center of the apical membrane; in RhoAV14 cells, GP135 was almost absent from the apical membrane and was instead localized in the lateral membrane and intracellular structures (Fig. 7).

With the exception of Rac1N17 cells, in which the defect in GP135 organization was mild, abnormalities in GP135 and F-actin organizations at the apical membrane coincided in Rac1V12 and RhoAV14 cells. The organization of actin at the apical membrane is structurally complex and very different from that at other membrane domains. A bundle of actin filaments is attached to the tip of each mi-

crovillus and inserts into the terminal web of actin filaments and associated proteins located beneath the apical membrane (Mooseker, 1985). The fine, granular staining pattern of GP135 in control cells reflects the organization of short microvilli on the apical surface, and disruptions in this pattern may, therefore, reflect changes in microvillar actin organization. The location of the intracellular aggregate of GP135 and F-actin in Rac1V12 cells is reminiscent of the apical recycling compartment or endosome that has been described previously (Apodaca et al., 1994;Odorizzi et al., 1996). This recycling endosomal compartment receives transcytotic vesicles from the basal–lateral membrane and endocytic vesicles internalized from the apical membrane, and it sends out vesicles to the apical membrane. It is possible that Rac1V12 inhibited either GP135 delivery from the Golgi to the apical membrane or the recycling of internalized GP135 back to the apical membrane, or that it increased the rate of internalization of GP135 from the apical membrane. Note that we also showed that the vesicular aggregate containing GP135 and Rac1V12 colocalized with rab11 (Fig. 8), which may be involved in regulating vesicle traffic to or from endosomal compartments (Lazar et al., 1997; Novick and Zerial, 1997). Although it is not known if Rac1 plays a role in direct vesicle transport from the Golgi to the plasma membrane, it has been shown to affect endocytosis (Lamaze et al., 1996), which, at the apical membrane in MDCK cells, is actin dependent (Gottlieb et al., 1993). The apparent mislocalization of GP135 to lateral membranes in RhoAV14 cells (Fig. 7 *B*) may reflect mistargeting of GP135 from the Golgi or loss of the tight junction fence to GP135 diffusion from the apical to the lateral membrane. However, results reported in the accompanying study (Jou et al., 1998) indicate that the latter possibility is unlikely. Further studies will be required to identify the defect in GP135 trafficking in these cells.

In summary, our analysis indicates that RhoA and Rac1 play important roles in the transition of epithelial cells from a motile, fibroblastic morphology to a static, polarized epithelium. This transition coincides with changes in the organization of the actin cytoskeleton. RhoA appears to regulate actin stress fibers at the basal membrane that are characteristic of single, motile cells. As RhoA mutants dominate (subsequent) Rac1 effects, RhoA-controlled fibroblastic structures may represent a ground state from which epithelial structures are built. Initiation of cell–cell contact leads to the formation of new actin structures and the specialization of lateral and apical membranes. Although RhoA may play an additional role during this reorganization (Jou et al., 1998), Rac1 activity appears to be required to assemble circumferential actin structures at the lateral membrane and actin structures associated with microvilli at the apical membrane, which affect the distributions of actin-associated membrane proteins.

We are very grateful to the following colleagues who made various reagents available to us: Dr. Rong-Guo Qiu (Onyx Pharmaceutical) for the RhoA and Rac1 mutant plasmids; Dr. Marc Symons and Dr. Bonnee Rubinfeld (Onyx Pharmaceutical) for Glu-Glu tagged RhoAV14, RhoAN19, Rac1V12, and Rac1N17 cDNA; Dr. George Cann (Stanford University) for mouse anti-myc hybridoma, 9E10; Dr. George Ojakian (SUNY Brooklyn) for the anti-GP135 hybridoma; and Dr. James Goldenring (Medical College of Georgia) for advice on rab11 staining and distribution. We thank members of the Nelson laboratory and Marc Symons (Onyx Pharmaceutical) for their criticisms and help during the course of this work.

This work was supported by a grant from the National Institutes of Health to W.J. Nelson.

Received for publication 16 March 1998 and in revised form 27 May 1998.

References

Amano, M., M. Ito, K. Kimura, Y. Fukata, K. Chihara, T. Nakano, Y. Matsuura, and K. Kaibuchi. 1996. Phosphorylation and activation of myosin by Rho-associated kinase (Rho-kinase). *J. Biol. Chem.* 271:20246–20249.

Apodaca, G., L.A. Katz, and K.E. Mostov. 1994. Receptor-mediated transcytosis of IgA in MDCK cells is via apical recycling endosomes. *J. Cell Biol.* 125: 67–86.

Barth, A.I., A.L. Pollack, Y. Altschuler, K.E. Mostov, and W.J. Nelson. 1997. NH_2-terminal deletion of β-catenin results in stable colocalization of mutant β-catenin with adenomatous polyposis coli protein and altered MDCK cell adhesion. *J. Cell Biol.* 136:693–706.

Bourne, H.R. 1993. GTPases. A turn-on and a surprise. *Nature.* 366:628–629.

Braga, V.M., L.M. Machesky, A. Hall, and N.A. Hotchin. 1997. The small GTPases Rho and Rac are required for the establishment of cadherin-dependent cell–cell contacts. *J. Cell Biol.* 137:1421–1431.

Burridge, K., and W.M. Chrzanowska. 1996. Focal adhesions, contractility, and signaling. *Annu. Rev. Cell Dev. Biol.* 12:463–518.

Burridge, K., M. Chrzanowska-Wodnicka, and C. Zhong. 1997. Focal adhesion assembly. *Trends Cell Biol.* 7:342–347.

Chen, J., J.A. Cohn, and L.J. Mandel. 1995. Dephosphorylation of ezrin as an early event in renal microvillar breakdown and anoxic injury. *Proc. Natl. Acad. Sci. USA.* 92:7495–7499.

Chong, L.D., K.A. Traynor, G.M. Bokoch, and M.A. Schwartz. 1994. The small GTP-binding protein Rho regulates a phosphatidylinositol 4-phosphate 5-kinase in mammalian cells. *Cell.* 79:507–513.

Eaton, S., P. Auvinen, L. Luo, Y.N. Jan, and K. Simons. 1995. CDC42 and Rac1 control different actin-dependent processes in the *Drosophila* wing disc epithelium. *J. Cell Biol.* 131:151–164.

Friederich, E., C. Huet, M. Arpin, and D. Louvard. 1989. Villin induces microvilli growth and actin redistribution in transfected fibroblasts. *Cell.* 59: 461–475.

Fukami, K., K. Furuhashi, M. Inagaki, T. Endo, S. Hatano, and T. Takenawa. 1992. Requirement of phosphatidylinositol 4,5-bisphosphate for α-actinin function [see comments]. *Nature.* 359:150–152.

Goldschmidt, C.P., L.M. Machesky, J.J. Baldassare, and T.D. Pollard. 1990. The actin-binding protein profilin binds to PIP2 and inhibits its hydrolysis by phospholipase C. *Science.* 247:1575–1578.

Gossen, M., and H. Bujard. 1992. Tight control of gene expression in mammalian cells by tetracycline-responsive promoters. *Proc. Natl. Acad. Sci. USA.* 89:5547–5551.

Gottlieb, T.A., I.E. Ivanov, M. Adesnik, and D.D. Sabatini. 1993. Actin microfilaments play a critical role in endocytosis at the apical but not the basolateral surface of polarized epithelial cells. *J. Cell Biol.* 120:695–710.

Hall, A. 1998. Rho GTPases and the actin cytoskeleton. *Science.* 279:509–514.

Hawkins, P.T., A. Eguinoa, R.-G. Qiu, D. Stokoe, F.T. Cooke, R. Walters, S. Wennstrom, L. Claesson-Welsh, T. Evans, M. Symons, and L. Stephens. 1995. PDGF stimulates an increase in GTP-Rac via activation of phosphoinositide 3-kinase. *Cur. Biol.* 5:393–403.

Hordijk, P.L., J.P. ten Klooster, R.A. van der Kammen, F. Michiels, L.C. Oomen, and J.G. Collard. 1997. Inhibition of invasion of epithelial cells by Tiam1-Rac signaling. *Science.* 278:1464–1466.

Ishizaki, T., M. Maekawa, K. Fujisawa, K. Okawa, A. Iwamatsu, A. Fujita, N. Watanabe, Y. Saito, A. Kakizuka, N. Morii, and S. Narumiya. 1996. The small GTP-binding protein Rho binds to and activates a 160-kD Ser/Thr protein kinase homologous to myotonic dystrophy kinase. *EMBO (Eur. Mol. Biol. Organ.) J.* 15:1885–1893.

Jou, T.-S., E.E. Schneeberger, and W.J. Nelson. 1998. Structural and functional regulation of tight junctions by RhoA and Rac1 Small GTPases. *J. Cell Biol.* 142:101–115.

Kaiser, H.W., E. O'Keefe, and V. Bennett. 1989. Adducin: Ca^{++}-dependent association with sites of cell–cell contact. *J. Cell Biol.* 109:557–569.

Kimura, K., M. Ito, M. Amano, K. Chihara, Y. Fukata, M. Nakafuku, B. Yamamori, J. Feng, T. Nakano, K. Okawa, et al. 1996. Regulation of myosin phosphatase by Rho and Rho-associated kinase (Rho-kinase). *Science.* 273: 245–248.

Kimura, K, Y. Fukata, Y Matsuoka, V. Bennett, Y. Matsuura, K. Okawa, A. Iwamatsu, and K. Kaibuchi. 1998. Regulation of the association of adducin with actin filaments by Rho-associated kinase (Rho-kinase) and myosin phosphatase. *J. Biol. Chem.* 273:5542–5548.

Lamaze, C., T.H. Chuang, L.J. Terlecky, G.M. Bokoch, and S.L. Schmid. 1996. Regulation of receptor-mediated endocytosis by Rho and Rac. *Nature.* 382: 177–179.

Lassing, I., and U. Lindberg. 1985. Specific interaction between phosphatidylinositol 4,5-bisphosphate and profilactin. *Nature.* 314:472–474.

Laza, T., M. Gotte, and D. Gallwitz. 1997. Vesicular transport: how many Ypt/Rab-GTPases make a eukaryotic cell? *Trends Biochem. Sci.* 22:468–472.
Leung, T., E. Manser, L. Tan, and L. Lim. 1995. A novel serine/threonine kinase binding the Ras-related RhoA GTPase which translocates the kinase to peripheral membranes. *J. Biol. Chem.* 270:29051–29054.
Leung, T., X.Q. Chen, E. Manser, and L. Lim. 1996. The p160 RhoA-binding kinase ROK alpha is a member of a kinase family and is involved in the reorganization of the cytoskeleton. *Mol. Cell. Biol.* 16:5313–5327.
Marrs, J.A., E.W. Napolitano, C. Murphy-Erdosh, R.W. Mays, L.F. Reichardt, and W.J. Nelson. 1993. Distinguishing roles of the membrane–cytoskeleton and cadherin-mediated cell–cell adhesion in generating different Na^+, K^+-ATPase distributions in polarized epithelia. *J. Cell Biol.* 123:149–164.
Matsui, T., M. Amano, T. Yamamoto, K. Chihara, M. Nakafuku, M. Ito, T. Nakano, K. Okawa, A. Iwamatsu, and K. Kaibuchi. 1996. Rho-associated kinase, a novel serine/threonine kinase, as a putative target for small GTP binding protein Rho. *EMBO (Eur. Mol. Biol. Organ.) J.* 15:2208–2216.
Matsui, T., M. Maeda, Y. Doi, S. Yonemura, M. Amano, K. Kaibuchi, S. Tsukita, and S. Tsukita. 1998. Rho-Kinase phosphorylates COOH-terminal threonines of ezrin/radixin/moesin (ERM) proteins and regulates their head-to-tail association. *J. Cell Biol.* 140:647–657.
Mooseker, M.S. 1985. Organization, chemistry, and assembly of the cytoskeletal apparatus of the intestinal brush border. *Annu. Rev. Cell Biol.* 1:209–241.
Nobes, C.D., and A. Hall. 1995. Rho, rac, and cdc42 GTPases regulate the assembly of multimolecular focal complexes associated with actin stress fibers, lamellipodia, and filopodia. *Cell.* 81:53–62.
Novick, P., and M. Zerial. 1997. The diversity of Rab proteins in vesicle transport. *Curr. Opin. Cell Biol.* 9:496–504.
Nusrat, A., M. Giry, J.R. Turner, S.P. Colgan, C.A. Parkos, D. Carnes, E. Lemichez, P. Boquet, and J.L. Madara. 1995. Rho protein regulates tight junctions and perijunctional actin organization in polarized epithelia. *Proc. Natl. Acad. Sci. USA.* 92:10629–10633.
Odorizzi, G., A. Pearse, D. Domingo, I.S. Trowbridge, and C.R. Hopkins. 1996. Apical and basolateral endosomes of MDCK cells are interconnected and contain a polarized sorting mechanism. *J. Cell Biol.* 135:139–152.
Ojakian, G.K., and R. Schwimmer. 1988. The polarized distribution of an apical cell surface glycoprotein is maintained by interactions with the cytoskeleton of Madin-Darby canine kidney cells. *J. Cell Biol.* 107:2377–2387.
Qiu, R.G., J. Chen, D. Kirn, F. McCormick, and M. Symons. 1995*a*. An essential role for Rac in Ras transformation. *Nature.* 374:457–459.
Qiu, R.G., J. Chen, F. McCormick, and M. Symons. 1995*b*. A role for Rho in Ras transformation. *Proc. Natl. Acad. Sci. USA.* 92:11781–11785.
Ridley, A.J., and A. Hall. 1992. The small GTP-binding protein rho regulates the assembly of focal adhesions and actin stress fibers in response to growth factors. *Cell.* 70:389–399.
Ridley, A.J., H.F. Paterson, C.L. Johnston, D. Diekmann, and A. Hall. 1992. The small GTP-binding protein rac regulates growth factor-induced membrane ruffling. *Cell.* 70:401–410.
Symons, M. 1996. Rho family GTPases: the cytoskeleton and beyond. *Trends Biochem. Sci.* 21:178–181.
Takaishi, K., T. Sasaki, H. Kotani, H. Nishioka, and Y. Takai. 1997. Regulation of cell–cell adhesion by rac and rho small G proteins in MDCK cells. *J. Cell Biol.* 139:1047–1059.
Takeichi, M. 1991. Cadherin cell adhesion receptors as a morphogenetic regulator. *Science.* 251:1451–1455.
Yao, X., and J.G. Forte. 1996. Membrane–cytoskeleton interaction in regulated exocytosis and apical insertion of vesicles in epithelial cells. *Curr. Top. Membr.* 43:73–96.